

Quantifying excitations of quasinormal mode systems

Hans-Peter Nollert

Astronomy and Astrophysics, University of Tübingen, 72076 Tübingen, Germany

Richard H. Price

Department of Physics, University of Utah, Salt Lake City, UT 84112

Computations of the strong field generation of gravitational waves by black hole processes produce waveforms that are dominated by quasinormal (QN) ringing, a damped oscillation characteristic of the black hole. We describe here the mathematical problem of quantifying the QN content of the waveforms generated. This is done in several steps: (i) We develop the mathematics of QN systems that are complete (in a sense to be defined) and show that there is a quantity, the "excitation coefficient," that appears to have the properties needed to quantify QN content. (ii) We show that incomplete systems can (at least sometimes) be converted to physically equivalent complete systems. Most notably, we give a rigorous proof of completeness for a specific modified model problem. (iii) We evaluate the excitation coefficient for the model problem, and demonstrate that the excitation coefficient is of limited utility. We finish by discussing the general question of quantization of QN excitations, and offer a few speculations about unavoidable differences between normal mode and QN systems.

PACS numbers: 02.10.Sp, 02.30.Lt, 04.30.Db, 04.70.s

I. INTRODUCTION AND OUTLINE

Essentially all computations of the generation of gravitational waves by strong field black hole processes produce a gravitational wave with the shape of a damped sinusoid [1]. The oscillation period and damping time depend only on the parameters of the black hole, and not on the manner of excitation. The meaning of the complex frequency of this damped oscillation is now well understood. A single frequency perturbation outside the hole can satisfy the natural radiative boundary conditions (radiation into the black hole and outward to infinity) only if the frequency is one of the discrete set of frequencies, called quasinormal (hereafter QN) frequencies. The least damped of these complex frequencies is what dominates the appearance of computed waveforms.

QN excitations are relevant, in principle, to most or all systems with radiative boundary conditions. Stellar models for example have short periods for nonradial oscillations driven by fluid pressures, and long damping times of these fluid oscillations due to the weak emission of gravitational waves. The motions of the stellar fluid can be studied with radiation damping omitted (e.g., with the use of Newtonian gravitation theory, or Post-Newtonian theory) and the weak radiation can be added, after the fact. When the radiative coupling is "turned on" the problem of the oscillation of a perfect fluid stellar model can be analyzed in normal modes [2,3] and one can find the radiated energy coming from each separate oscillation frequency, and can decompose the radiative power into that fraction assigned to each frequency.

The situation is dramatically different for black holes, which have only a single time scale. (For a nonrotating hole this is $2GM/c^3$ where G is the universal gravitational constant, c is the speed of light, and M is the mass of the hole.) The period and damping time are therefore of the same order and there is no meaningful way of turning on the damping for black hole oscillations; there is no underlying normal mode system. This suggests that there may be no clear way of specifying "how much QN ringing" of some particular black hole QN frequency is contained in an emitted waveform. This suggestion is made plausible by the mathematical origins of normal modes and QN modes. The properties and usefulness of normal modes are closely related to the fact that they are eigensolutions to a self adjoint problem. QN modes, on the other hand, are eigensolutions of a problem that is not self adjoint. But the dominance of QN frequencies in computed waveforms is so robust that it seems that the strength of QN ringing must be quantifiable, or at least that mathematical sense must be made of the question.

In this paper we try to make mathematical sense of quantification. In attempting this we draw upon parallels with normal modes systems. By the "excitation" of a mode we mean, in parallel to excitation in normal modes systems, an index of the contribution that each mode makes to the overall waveform and to the energy. To develop a description of QN excitation we start with a viewpoint that a meaningful and rigorous quantification is very implausible unless the QN system is, in some sense, complete. We then follow a three step process. First, in Sec. II, we define and posit the existence of QN systems that are complete (in a sense to be defined). We then point out difficulties in quantifying excitation in a complete QN system. We construct a particular measure, the "excitation coefficient" that overcomes these difficulties, and is closely related to the description of the excitation of normal modes.

Our next step is to prove the existence of complete QN systems and relate the mathematics of black hole processes to complete systems. This step, carried out in Sec. III requires a rather lengthy discussion of "induced completeness." Though this discussion is not directly related to the problem of QN excitation, it is a necessary step (and is interesting in its own right). The discussion in Sec. III shows that completeness can be induced. That is, an incomplete QN system can be changed with a modification that satisfies two criteria: (i) The effect of the modification can be made arbitrarily weak. More specifically, the modification can be made small enough so that the waveform that evolves from any initial conditions is arbitrarily close to the waveform evolving with no modification. (ii) No matter how weak the modification is, the modified QN system is complete. Our demonstration in Sec. III does not consist of a general theory for such modifications; a conjecture about the general conditions has been given by Young et al. [4] (though their definition of completeness is somewhat different from ours). Here we will sacrifice generality and direct astrophysical relevance for specificity and rigor. We present the details of a specific model. We will start with a model, the "TDP" with only a single conjugate pair of QN frequencies, and modify it to the "spiked TDP," a model with an infinite QN spectrum. The Appendix gives a rigorous proof of completeness of the spiked TDP (i.e., that under specified circumstances the outgoing waveform is a convergent sum of components at quasinormal frequencies). Numerical results are shown in Sec. III to demonstrate the negligible effect of the modification, and to demonstrate the pattern of convergence of sums of single frequency excitations.

Having established that completeness can be induced (at least in one model problem), we return, in Sec. IV, to the question of measuring the excitation of QN modes and in particular to the excitation coefficient, introduced in Sec. II. We demonstrate, with a few examples, that this formal measure of excitation does not generally give a useful quantification. The failure of this measure is discussed along with a broader discussion of differences between QN and normal mode systems, and conjectures about mathematical properties of QN systems.

II. COMPLETE QN SYSTEMS

A. Definition of QN frequencies

For definiteness we will limit considerations to solutions of the equation

$$\frac{\partial^2}{\partial x^2} - \frac{\partial^2}{\partial t^2} - V(x) = 0 : \quad (1)$$

Such an equation describes the dynamics of many mechanical systems, and the evolution of multipole perturbations (scalar, electromagnetic, or gravitational) of spherically symmetric (Schwarzschild) black holes [5,7]. Perturbations of rotating (Kerr) holes [7], on the other hand, cannot be reduced to radial-time equations. QN oscillations are single frequency solutions of the form $\psi(t;r) = \psi(x) \exp(i\omega t)$ and hence are solutions of the equation

$$\frac{\partial^2}{\partial x^2} + \omega^2 - V(x) = 0 : \quad (2)$$

We assume that the domain of x includes $x = 1$, and that the nature of the potential $V(x)$ is such that a "radiative boundary condition" can be defined at $x \rightarrow 1$. A clear example is a potential with support of $V(x)$ only for x less than some x_{max} . In this case the boundary condition is that $\psi(x) \sim \exp(-i\omega x)$ for $x > x_{\text{max}}$.

For potentials that do not vanish, but fall off sufficiently fast as $x \rightarrow 1$, the more general radiative boundary condition for real frequencies will be that for large x , the solution for $\psi(x)$ have the form $\exp(-i\omega x)F(\omega; x)$, with $F(\omega)$ constant, as $x \rightarrow 1$. This condition is not quite sufficient if ω has a positive imaginary part; see [8] for a complete discussion. In short, the solution satisfying a radiative boundary condition for complex ω can be regarded as an analytical continuation of a solution satisfying a radiative boundary condition for real ω .

The boundary condition at the other end of the x domain may be a standard Sturm-Liouville boundary condition (e.g., $\psi = 0$ at $x = 0$) or may be a radiative boundary condition at $x \rightarrow 1$. For spherically symmetric black holes, the range of x extends from r_1 to 1 , with r_1 representing the black hole horizon [8,9]. The potentials fall off exponentially in x as $x \rightarrow 1$ and as $\text{const} \cdot x^2$, as $x \rightarrow 1$. Radiative boundary conditions are imposed both at $x \rightarrow 1$ and $x \rightarrow 1$, corresponding to radiation moving inward through the black hole horizon, and outward towards spatial infinity.

QN frequencies, are the eigenvalues $\omega = \omega_{\text{QN}}$ to the problem defined by (2) for radiative boundary conditions of the type just discussed. Due to the boundary conditions, this problem is generally not of the Sturm-Liouville type and the usual features of eigenvalues of a Sturm-Liouville problem are absent. In particular the QN frequencies ω_{QN} are generally not real. A positive imaginary part indicates an exponential decrease with time. A negative imaginary part would indicate an instability; no frequencies with negative imaginary parts have been found for black hole QN systems.

It is clear that QN frequencies must occur in conjugate pairs. If ω_{QN} is a solution to the eigenproblem corresponding to ω_{QN} , then $\bar{\omega}_{\text{QN}}$ is also a solution corresponding to $\bar{\omega}_{\text{QN}}$. We will use a tilde (\sim) to denote the conjugate relationship of QN frequencies. Thus the conjugate to QN frequency ω_{γ} is $\tilde{\omega}_{\gamma}$, that is $\tilde{\omega}_{\gamma} = \bar{\omega}_{\gamma}$.

B. Definition of completeness

We will choose to give a rather specific meaning to a complete system of QN modes. The Cauchy data for (1) consists of ψ_0 and $\dot{\psi}_0$, the initial value of ψ and of its time derivative,

$$\psi_0(x) = \psi(t; x)|_{t=0}, \quad \dot{\psi}_0(x) = \partial_t \psi(t; x)|_{t=0} \quad (3)$$

We consider an interval $x_2 < x < x_1$ in the domain of x and we consider Cauchy data at $t = 0$ for (1) which has support only in this interval. We then consider the solutions to (1) for such data, and we focus attention on the value of this solution at x_{obs} , a particular value of x satisfying $x_{\text{obs}} > x_1$. This corresponds to the physical situation of an observer at x_{obs} detecting radiation resulting from an initial disturbance located at some distance from her. The "observed waveform" that we focus on is then

$$f(t) = \psi(x_{\text{obs}}; t) : \quad (4)$$

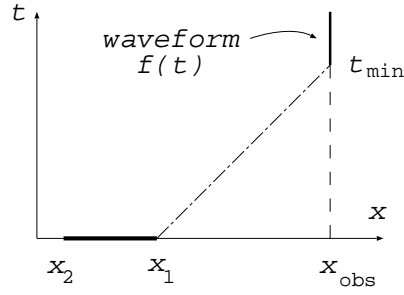


FIG. 1. Propagation of initial data to the observation location x_{obs} defining the waveform $f(t)$.

As shown in Fig. 1, there will in general be a minimum value t_{min} of t , such that the point x_{obs}, t is influenced by the evolved Cauchy data. That is, for $t < t_{\text{min}}$, the area between the past directed characteristics from $t; x_{\text{obs}}$ intersects the $t = 0$ hypersurface outside the support of the Cauchy data. We are interested in $f(t)$ only for $t \geq t_{\text{min}}$. The physical interpretation of this is that we are considering only the waveform generated by the Cauchy data.

We take a complete QN system to be one which satisfies the following criteria:

The solutions to the QN eigenvalue problem form a discrete spectrum and can be arranged in order of increasing $j(\ell_n)$.

We consider only Cauchy data that

{ has support only within a compact region $[x_2; x_1]$.

{ belongs to a specific continuity class C^p , where p depends on the nature of the problem.

{ results in a waveform which is square integrable from $t = t_{\text{min}}$ to 1 .

For such Cauchy data, the waveform $f(t)$ that evolves from any such allowed Cauchy data can be written as

$$f(t) = \sum_n a^n e^{i\ell_n t} : \quad (5)$$

Here a^n is the n^{th} coefficient in the sum over QN modes. Since $f(t)$ is a function of x_{obs} , the a^n coefficients are also functions of x_{obs} , but we shall not explicitly exhibit this dependence. The summation in (5) is in order of increasing $j(\ell_n)$ and the convergence is uniform for $t > t_{\text{min}}$.

It is important to note that our view of completeness is rather different from other possible meanings of the term. In particular, our choice of the meaning of completeness has nothing directly to do with the x -dependence of the single frequency solutions and with the question of whether these solutions can be used to span acceptable Cauchy data. Our meaning of completeness, then, is rather different from that of Young et al. [4]. It also disagrees with the concept of completeness used by Husain and Price [10] and by Beyer [2], and Beyer and Schmidt [3].

C. Function space and inner product

In accordance with our definition of completeness, our vector space is the space of all functions $f(t); t \geq t_{\text{min}}$ that can evolve from acceptable Cauchy data. Our class of acceptable Cauchy data will always be chosen so that $f(t)$ is square integrable from $t = t_{\text{min}}$ to 1 . On this space of functions we define an inner product to be:

$$(f, g) = \int_{t_{\text{min}}}^1 f(t)g(t) dt : \quad (6)$$

We could of course include a weight function $W(t \geq t_{\text{min}})$ in the integral defining the inner product, but the time translational symmetry of the background suggests that W should be constant. The choice in Eq. (6), furthermore, means that (f, f) is the time integral of the square of the wave function, a measure closely related to the energy content of a wave. (For black hole processes, the connection with gravitational wave power will be made explicit presently.) Our assumption of completeness above means that the functions $\exp(i\ell_n t)$, while not elements of our function space themselves, span this function space in the sense of (5); we will therefore consider them a basis. For a function $f(t)$ in our space we can use the inner product to compute another set of coefficients a_n by

$$a_n = \int_{t_{\text{min}}}^{t_{\text{max}}} e^{i\omega_n t} f(t) dt : \quad (7)$$

The following relations for the coefficients of conjugate modes are straightforward to verify:

$$a_k^* = (a_k) \quad a^k = (a^k) \quad (8)$$

Since the convergence is uniform by hypothesis, we can integrate term by term in the sum-of-modes expression for the norm of f to find:

$$\int_{t_{\text{min}}}^{t_{\text{max}}} f(t) \bar{f}(t) dt = \int_{t_{\text{min}}}^{t_{\text{max}}} \sum_n a^n e^{i\omega_n t} \bar{f}(t) dt = \sum_n (a^n)^* a_n : \quad (9)$$

The final sum in (9) is real, as it must be, since for any k , the sum $(a^k)^* a_k + (a^k) a_k^*$ is real.

In most physical problems the radiated power is the square of the time derivative of the waveform. If at x_{obs} our wave function evolving from the initial data is $f(t) = \psi(x_{\text{obs}}; t)$. If $f(t_{\text{min}})$ vanishes (i.e., if the waveform starts continuously) then this type of energy can be evaluated as

$$\int_{t_{\text{min}}}^{t_{\text{max}}} \dot{f}(t)^2 dt = \sum_n (\omega_n)^2 (a^n)^* a_n : \quad (10)$$

As in (9) the reality of the sum is guaranteed by the relations of conjugate coefficients in (8).

Since we have an inner product, we have an equivalence between vectors and dual vectors in our function space and we can define a set of covariant basis functions $\bar{e}^m(t)$ by the property $\bar{e}^m(t) e^{i\omega_n t} = \delta_{nm}$. It follows from Eq. (7) that the a_n are the expansion coefficients for $f(t)$ with respect to the covariant basis functions $e^{i\omega_n t}$. We shall henceforth refer to a^n and a_n , respectively, as the contravariant and covariant coefficients of $f(t)$. The components of the metric, in this function space, with respect to the QN basis, are

$$e^{i\omega_n t} e^{i\omega_k t} = \int_{t_{\text{min}}}^{t_{\text{max}}} e^{i(\omega_k - \omega_n)t} dt = G_{nk} : \quad (11)$$

It should be noted that G is a hermitian matrix, but it is not diagonal, i.e., the QN oscillations are not orthogonal. The metric coefficients can be used, in principle, to relate a^n and a_n . The expression for $f(t)$ in Eq. (5) can be substituted in Eq. (7). Since the convergence in Eq. (5) is uniform, we can integrate term by term and get

$$a_n = \sum_k G_{nk} a^k : \quad (12)$$

Since G_{nk} is not diagonal, the covariant basis vectors, i.e., the basis vectors dual to $e^{i\omega_n t}$, are mixtures of the $e^{i\omega_n t}$ functions (usually involving all of them). An indication of the unfamiliar problems this produces can be seen in the following rough argument. Let us suppose that we have a waveform that in some sense is "almost pure" (say) seventh mode. That is, suppose that $f(t) = a^7 e^{i\omega_7 t} + a^7 e^{i\omega_7 t}$. (We are supposing that this relationship is only approximate since it will in general be impossible to excite a truly pure single frequency mode with smooth, compact initial data.) This waveform, for which (almost) the only contravariant coefficients are a^7 and a^7 , will have contravariant coefficients a^n for all n . A waveform that is a pure (or almost pure) single mode excitation in one sense is therefore not a single mode excitation in another. This presages some of the problems in quantifying the excitation of a mode, and we will return to this point at the end of Sec. IV.

It is possible, of course, to use Gram-Schmidt orthogonalization to find basis functions which are orthogonal according to the inner product of (6). The resulting basis functions will not (except for one of them) correspond to single frequency excitations, and do not seem to be of interest.

D. Intuitive insights; the excitation coefficient

Some rough considerations of mode problems suggest the intuitive basis for some of the mathematical difficulties to appear below, and point to a possible approach to quantifying excitation. The most obvious difficulty is the "time shift" problem. We imagine a configuration like that pictured in Fig. (2): A potential with compact support and two sets of Cauchy data (a) and (b). The two Cauchy data sets are localized and are identical except that set (b) is

shifted to the left, to smaller x , by some finite displacement Δx . The support of neither Cauchy data set overlaps the support of the potential. In this case it is clear that the waveform generated from the two cases will be identical except that the waveform from (b) will be shifted to later times, relative to that for (a), by an amount $\Delta t = \Delta x$. Each contravariant coefficient will therefore be larger in the (b) waveform than in the (a) waveform. The conjugate pair of contravariant coefficients $f_{a^7}; a^7_g$ will, for example, be larger by $\exp[(=!) \Delta t]$ for (b) than for (a), though the excitation is physically identical. The analogous difficulty does not arise for normal modes; since they are not damped, the time delay only causes a phase shift. The trend is opposite for the covariant coefficients $f_{a_7}; a_7_g$. As deduced in (7) $f_{a_7}; a_7_g$ will be smaller for (b), since $\exp(-i!) \Delta t$ (or $\exp(-i!) \Delta t$) are smaller by $\exp[(=!) \Delta t]$ at the later times during which the (b) waveform has support. Therefore, neither the coefficients a^k nor a_k alone can provide a useful measure for the excitation of a QN mode.

Any useful measure of excitation must give the same result for the two waveforms in Fig. (2). We take advantage of the opposite tendencies of the contravariant and covariant coefficients under time shift to define a quantity that is the same for both waveforms, the "excitation coefficient" A_k for the k^{th} QN mode:

$$A_k = (a_k) a^k + (a_k) a^k ; \quad (13)$$

We conjecture that these excitation coefficients, or quantities constructed from them (sums of excitation coefficients, functions of excitation coefficients, etc.) or quantities very closely related (see the energy excitation coefficient, below) are the only relevant mathematical objects in the vector space that are unaffected by the time shifts, and have the additional properties that we outline in the following.

In addition to the insensitivity of the excitation coefficient to time shifts of waveforms, the excitation coefficient has another important and relevant property (cf. Eq. (9)):

$$\int_{t_{\text{min}}}^{\infty} |f(t)|^2 dt = \sum_k A_k ; \quad (14)$$

where the sum is over conjugate pairs. The excitation coefficients of the complete set of QN modes sum to the norm of the waveform. We can define a quantity closely related to A_k :

$$E_k = (|!)^2 (a_k) a^k + (|!)^2 (a_k) a^k ; \quad (15)$$

We shall refer to the E_k as the energy excitation coefficient. According to (10), the sum over conjugate pairs of these coefficients gives the norm of f . The summation properties of the A_k and the E_k are important in clarifying what we mean by the "excitation" we are attempting to quantify. These coefficients appear to tell us the contribution made by each mode to a measure of the waveform. In the case of black hole perturbations it turns out that it is possible to make an even more direct connection. If $f(t)$ is a solution of the Zerilli equation [6] for even parity perturbations, then the integral on the left of (10) is proportional to the radiated energy and E_k has the appearance of the energy in the k^{th} mode. If $f(t)$ is a solution of the Regge-Wheeler equation [5] for odd parity perturbations, then the integral in Eq. (9) is the energy and A_k has the appearance of the energy in the k^{th} mode.

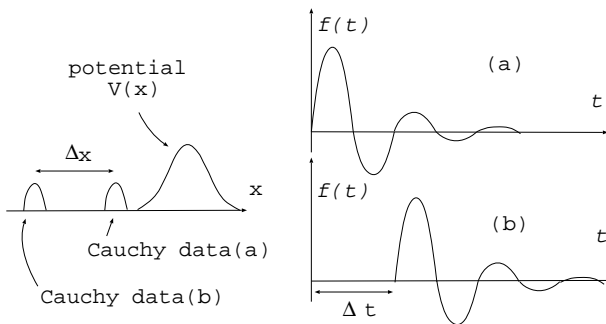


FIG. 2. Initial data shifted in location produces identical waveforms shifted in time.

The possibility of quantization with the excitation coefficient (or energy excitation coefficient) will be a central focus, of Sec. IV, but before we begin specific computations, there are a few more possibly useful insights that can be found from intuitive considerations. For one thing, it is interesting that the two sets of coefficients can be related to two different aspects of an emitted wave. The contravariant coefficients, telling us how much of a certain mode must be added in order to get the waveform, can be considered a "theoretical" coefficient. For a given waveform,

the projection operation on the waveform defined by (7) can be considered to give the "experimental" excitation coefficient.

Simple considerations can also produce insights into the nature of the metric matrix G_{nk} defined in (11). Consider the signal produced by some Cauchy data, and let the vector a denote the contravariant coefficients of the resulting waveform with respect to the QN mode basis. Let the vector of covariant coefficients be given by \underline{a} , so that $\underline{a} = G a$. Now consider the same Cauchy data, shifted to the left by x . The new contravariant and covariant coefficient vectors will be given by: $\tilde{a}^k = \exp(-i!_k x) a^k$ and $\tilde{a}_k = \exp(i!_k x) a_k$. Taking the standard linear algebra norm $\| \cdot \|$, we have $\| \tilde{a} \| = \| a \|$ and $\| \tilde{\underline{a}} \| = \| \underline{a} \|$ where > 1 and < 1 .

The exact magnitude of $\| \tilde{a} \|$ depends on the distribution of the contravariant coefficients and the shift x . In fact, we can always make the shift large enough so that $\| \tilde{a} \| > 1$. In the same way, we can ensure that $\| \tilde{\underline{a}} \| < 1$. Assuming that the metric matrix G has a minimum eigenvalue e_{\min} and a maximum eigenvalue e_{\max} , we then find:

$$e_{\min} = \frac{\| \tilde{\underline{a}} \|^2}{\| \tilde{a} \|^2} = \frac{\| \underline{a} \|^2}{\| a \|^2} \frac{\| \tilde{\underline{a}} \|^2}{\| \underline{a} \|^2} \quad e_{\max} : \quad (16)$$

Since G is an infinite dimensional matrix there need not be a maximum or a minimum eigenvalue. For the model problem introduced in Sec. III, we will give numerical evidence, in Sec. IV B, that the ratio of maximum and minimum eigenvalues diverges. The G matrix therefore is in some sense singular.

We now make the additional assumption that we have constructed Cauchy data such that the waveform consists almost exclusively of ringing in a single QN mode. (In the specific example discussed in the following sections, this will be possible for the fundamental mode using an arbitrarily short "burst" of initial data.) Let us modify the example of Fig. 2, by reducing the size of Cauchy data (b) by a factor $\exp(-!_1 x)$, so that once the response to the (b) data starts it is identical to that of the (a) response at the same time. This situation is shown in Fig. 3 in which the response $f(t)$ is the same in both plots for $t \geq t_s$.

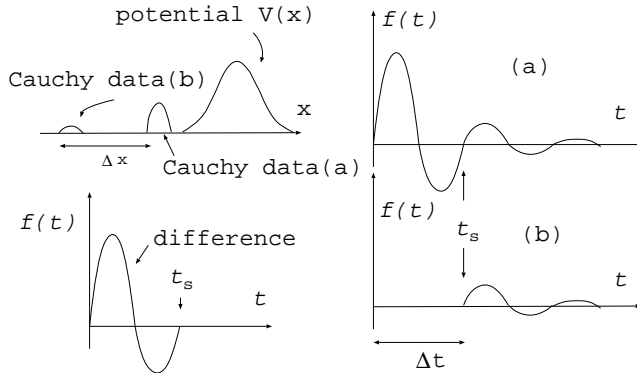


FIG. 3. Oscillations produced by shifting and scaling initial data.

Now let us suppose that the waveforms are dominated by ringing of the fundamental mode, and that $f(t)$ consists only of ringing of the fundamental mode. The difference between the two responses is a sum of QN modes which has the appearance of truncated fundamental mode ringing, but which has $a^1 = \tilde{a}^1 = 0$ in its mode sum. The time t_s can in principle be made arbitrarily long, so the truncation in the difference curve can be made arbitrarily late. We have then a sum of modes that looks arbitrarily close to fundamental mode ringing, but containing no fundamental mode. This suggests that the fundamental mode can "almost" be built as a superposition of the modes other than the fundamental mode, and that the modes are "almost" linearly dependent. We will discuss this further, based on numerical results, in Sec. IV C.

Again, this suggests that the infinite metric matrix G_{nk} is in some sense "almost" singular. A physical insight can be associated with this nature of the metric: Since G_{nk} is "almost singular" it is "almost noninvertible." This means that there are difficulties in finding the contravariant coefficients from the covariant coefficients, since this requires the inverse of G_{nk} . The implication of this is possibly of pragmatic importance: the near singularity makes it difficult to find the "theoretical" coefficients from the "experimental" ones.

III. INDUCED COMPLETENESS

A. Small change

Our approach to quantization of excitation is based on the idea of complete QN systems. It is important to demonstrate that complete QN systems exist and to have an example of a system in which we can compute excitation coefficients. We must also deal with a more specific issue. The QN modes of potentials for black hole problems do not form a complete set; both the Regge-Weeler potential, which describes perturbations of a Schwarzschild black hole, and the Pöschl-Teller potential [11], which has been used as an approximation to the black hole potential [12], have quasinormal mode sets which cannot completely describe the waveform resulting from an initial perturbation. An important question is what the relevance is to black hole processes, of any quantization based on an assumption of complete systems. The details of this section are somewhat disjoint from the main goal of the paper: quantization of QN excitation, but are a necessary step in developing our approach. (They are also rather interesting in their own right!)

The key idea in developing a demonstrably complete QN system, and in showing its relevance to black holes, is "induced completeness." It has been argued [4] that for the problem defined by (2), the eigenmodes will be complete if there are two values of x at which $V(x)$ is not C^1 . If this is true, it appears that the black hole potentials can be modified in such a way that completeness of QN oscillations is induced, while the effect on other aspects of the problem (in particular on the evolution of Cauchy data) is kept arbitrarily small. In this section we explore induced completeness.

It is not our purpose here to look into the generality of induced completeness. Rather, we want to have a specific example of a complete QN system with which to explore the question of quantifiability of QN excitations. We will therefore focus on a very specific model that contains most of the flavor of black hole potentials, but is simple enough to allow rather straightforward analysis and a proof of completeness.

We use the fact that (2) can be solved with elementary functions in the case that the potential has the form of a truncated centrifugal potential,

$$V_{TCP}(x) = \begin{cases} 0 & x < x_0 \\ \ell(\ell+1)/x^2 & x \geq x_0 \end{cases}; \quad (17)$$

where ℓ is an integer. It gives a good representation of the sharp cutoff of the black hole potential as $x \rightarrow 1$ and the approximate asymptotic form of the black hole potential at $x \rightarrow 1$. It differs from the true black hole potential in the details of the $x \rightarrow 1$ potential that give rise to the power-law late time tails of black hole waveforms. These tails almost certainly are an obstacle to an analysis of QN excitation, and a modification of the potential to eliminate these tails has already been made in work on QN excitation.

We will hereafter consider only the case $\ell = 1$, to be called the "truncated dipole potential" (TDP). An example of the simplicity of the TDP problem is that it has only a single pair of QN frequencies: $\omega_1 = (1+i)2x_0$ and $\omega_1^* = (-1+i)2x_0$ (see Appendix IA). There are several ways in which we could try to induce completeness into this problem. We have studied both the addition of a small step (with discontinuities) to the TDP and the addition of a delta function. The delta function has the disadvantage of its distributional nature, but it offers the advantage of considerable simplicity as compared with the step. We have found no significant "practical" difference between the results (QN locations, convergence of QN sums) between the two examples, so we will describe here completeness induced with a delta function. The total potential in this case will be called the "spiked truncated dipole potential" (STD P) and is given by

$$V_{STD P}(x) = V_{TDP}(x) + V(x - x_0); \quad (18)$$

where $V_{TDP}(x)$ is the $\ell = 1$ form of the potential in (17).

We first establish that the influence on the evolution of initial data can be made arbitrarily small. To do this we choose the Cauchy data, at $t = 0$ to be given by

$$\begin{aligned} \phi_0 &= \sin 2\pi \frac{x - x_0}{x_1 - x_0} & (\phi_0 = 0 \text{ at } x_1) \\ \phi_0' &= \phi_0' = 0 \end{aligned} \quad (19)$$

with $x_1 > x_0$, so that the initial data has the form of one full cycle of a sine wave, located to the left of the potential, traveling to the right. (This Cauchy data is chosen for convenience in demonstrating mathematical points; it has no justification as initial data for gravitational waves being produced in the neighborhood of a black hole.)

For the results to be shown here and in following sections, we choose $x_0 = 1$, $x_1 = 1.5$, $x_2 = 5$, and $x = 10$, and $x_{obs} = 120$. For this choice of x_1 and x_2 , the sine has a wavelength, 6, that is roughly half that of the QN oscillation

of the TDP. This allows us to see similar, but distinguishable signs in the evolved waveform of the propagation of the Cauchy data and of QN oscillation.

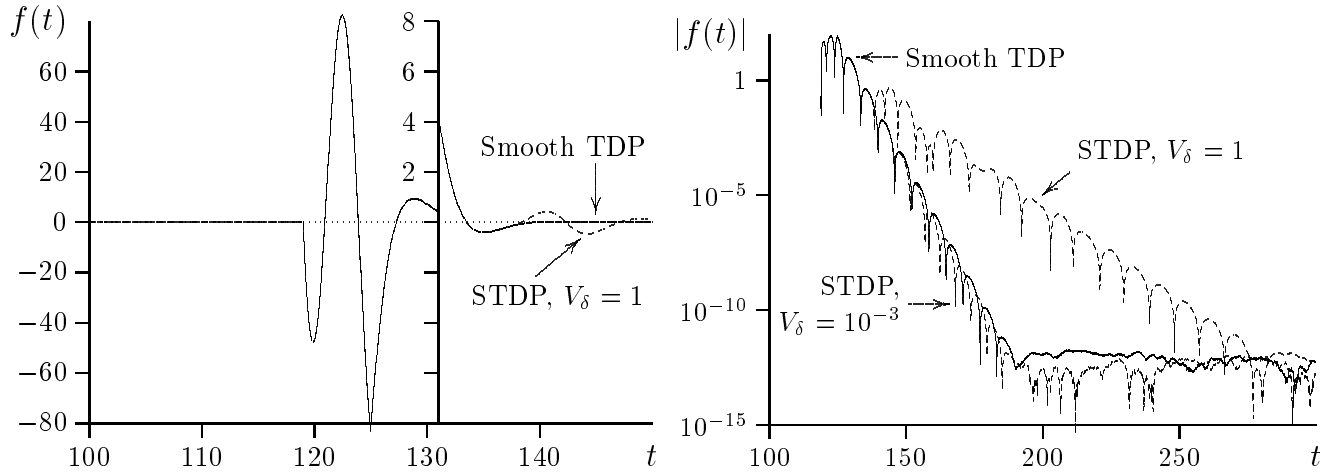


FIG. 4. Time evolution for initial data incident on the TDP and on the TDP with an added δ -function. Left: linear plot, right: logarithmic plot

Figure 4 shows the time evolution of the Cauchy data for the original TDP and for the TDP with an added δ -function with different amplitudes ranging from $V = 1$ to $V = 10^{-6}$. The waveforms are followed out to times at which they have decreased in magnitude from the maximum by a factor of 10^{15} , at which point numerical error obscures the results. Even for the largest value of V , the influence of the delta function on evolution is visible in the linear plot only after we change the scale for $f(t)$ at $t = 131$. To see the effects more clearly we also plot the logarithm of $|f(t)|$ for a longer observation time, showing several interesting features. For all but the largest amplitude of the delta function ($V = 1$) the waveform after the first few oscillations consists only of QN ringing, with the characteristic distance $t = j\pi/\omega_j = 2\pi/x_0 = 2$ between zeroes of $f(t)$. For $V = 10^{-3}$, the effect of the delta function shows up only as a phase shift after the first four, or so, full cycles of oscillation. The effect of the smallest delta function amplitude $V = 10^{-6}$ is smaller by two orders of magnitude than that for $V = 10^{-3}$, and too small to be seen even in the logarithmic plot of Fig. 4.

These results make it clear that any reasonable measure of the influence of the delta function, such as the integral of the square deviation from the TDP waveform, is tiny and decreases with decreasing V . We will accept these numerical results as a sufficient demonstration of this point, and will not attempt an analytic proof of this point.

B. QN spectra

Although the influence of a small delta function on the evolution of Cauchy data is negligible, the influence on the spectrum of QN frequencies is profound. The method of computing the QN frequencies for the STDP is outlined in Appendix I. The results of the computation are presented in Fig. 5 for the same potentials considered in Fig. 4.

The original TDP has only one pair of QN frequencies at $(1 \pm i) = 2$. With an added δ -function, an entirely new set of modes appear. Note that the real parts of the additional frequencies seem to be unbounded. The asymptotic spacing $\langle \omega_n \rangle = 2\pi/x_0 = 10$ of the real parts of the frequencies is shown in Appendix IC to correspond to the length of the "cavity" bounded by x_0 and the δ -function: $L = x_0 = 10$. The imaginary parts are shown in the Appendix to increase as the logarithm of the real part.

When V becomes sufficiently small, one of the QN frequencies approaches the value $(1 \pm i) = 2x_0$ of the "native" QN frequency, that of the original, TDP. This can be seen more clearly in Fig. 6, which shows the "path" of this QN frequency in the complex plane for values of V varying in steps of $1/2$ from $V = 1$ to $V = 10^{-6}$. As V decreases, the imaginary parts of the additional frequencies increase, moving them away from the native one, eventually leading to two very distinct subsets of QN frequencies.

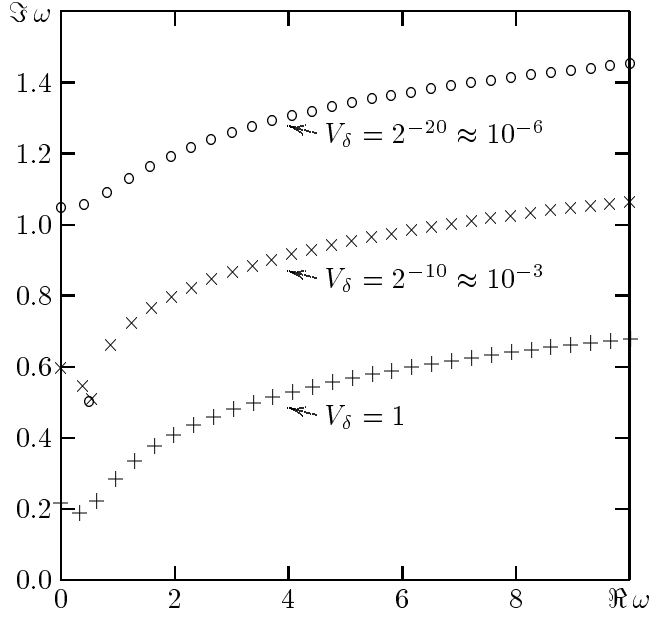


FIG. 5. Quasnormal frequencies for the TDP with an additional δ -function at $x = 10$.

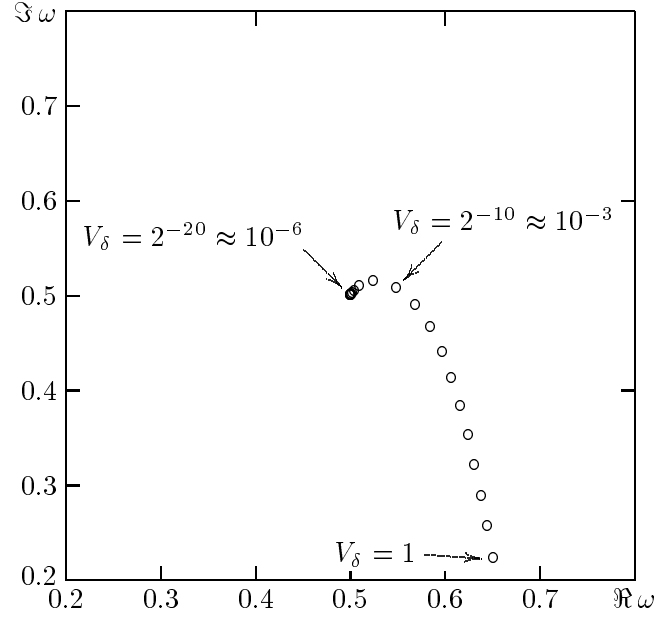


FIG. 6. Path of the original quasnormal frequency of the TDP as the amplitude of the additional δ -function is decreased.

It might seem that it is an obvious necessity for the QN spectrum to have a mode approximately at the location of the native mode, since the evolution of Cauchy data is only slightly affected. This turns out not to be true, however, for other ways of inducing apparent completeness [13]. Cutting off the TDP potential at some very large value of x , for example, has a negligible effect on the evolution of Cauchy data, and it also produces an unbounded set of additional QN frequencies. However, the spectrum of QN frequencies turns out to contain no frequency near the location of the native mode.

C. Complete sums

We now develop the connection between the Cauchy data ϕ_0 and ϕ_1 and the coefficients of QN oscillations (i.e., the contravariant components a^n in the case of complete QN bases). Here we simply outline how coefficients associated with QN basis functions are computed in general. In Appendix II a proof of completeness of sum with these coefficients will be given for the case of the spiked TDP, and of Cauchy data meeting certain criteria. One of the criteria will be compact support for the Cauchy data, and we will assume from the outset that ϕ_0 and ϕ_1 vanish outside the interval $x_2 < x < x_1$.

The QN coefficients are found by starting with a Laplace transform

$$\hat{\phi}(s; x) = \int_0^{x_1} e^{-st} \phi(t; x) dt : \quad (20)$$

(The connection between the Laplace variable s and the Fourier ω used in Appendix I and most of the paper, is through the correspondence $s \leftrightarrow i\omega$.) The transformed wave equation reads

$$(\partial_s^2 + V(x)) \hat{\phi}(s; x) = J(s; x) ; \quad (21)$$

in which the source $J(s; x)$ is determined by the Cauchy data:

$$J(s; x) = -\phi_1(x) - s \phi_0(x) \quad (22)$$

A solution can be found in the form

$$\hat{\phi}(s; x) = \int_{x_2}^{x_1} G(s; x; x^0) J(s; x^0) dx^0 : \quad (23)$$

Here the Green function can be constructed from the homogeneous solutions $f_-(s; x)$ and $f_+(s; x)$ of the wave equation (21):

$$G(s; x; x^0) = \frac{1}{W(s)} \begin{cases} f_-(s; x^0) f_+(s; x) & (x^0 < x); \\ f_-(s; x) f_+(s; x^0) & (x^0 > x); \end{cases} \quad (24)$$

where $W(s)$, the Wronskian of f_- and f_+ is independent of x and x^0 .

We will assume that the potential falls off quickly enough at $x \rightarrow \pm 1$ so that homogeneous solutions f_- and f_+ can be found with the property

$$f_-(s; x) \sim e^{sx} (1 + O(1/x)) \text{ as } x \rightarrow -1 \quad \text{and} \quad f_+(s; x) \sim e^{-sx} (1 + O(1/x)) \text{ as } x \rightarrow 1. \quad (25)$$

This condition is satisfied for black hole potentials and for the TDP.

Once we have found a solution of the Laplace transformed wave equation, we can reconstruct a solution of the time-dependent wave equation by applying the inverse Laplace transform:

$$(t; x) = \frac{1}{2\pi i} \int_{\Gamma} e^{st} \hat{\psi}(s; x) ds \quad (26)$$

where Γ denotes the path of integration, which lies parallel to and just to the right of the imaginary axis.

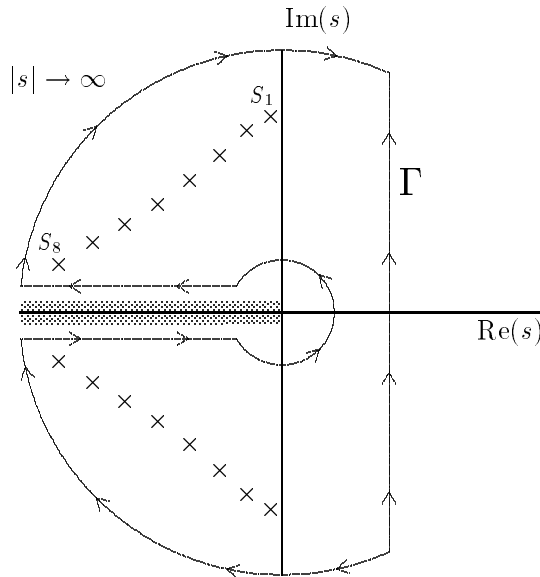


FIG. 7. Closing the contour for integration in the complex s plane. The curve Γ is the original contour of integration. It can be closed by the addition of an arc at infinity. If there is a branch point at the origin, as shown, then a branch cut can be drawn from $s = 0$ to $s = -1$, and the contour shown can be drawn.

Figure 7 illustrates features in the complex s plane. There may be poles and essential singularities, drawn as s_j , and there may be a branch point, like that shown at $s = 0$ in the figure. The contour Γ can be closed with the addition of a single arc to the left if $\hat{\psi}(s; x)$ is a single valued function of s to the left of ∞ . If there are branch points then a path like that shown in Fig. 7 must be used. The Green's function for the Regge-Wheeler potential has a branch point at $s = 0$, while the TDP and the STD P do not.

The integral for $\hat{\psi}$ may then be evaluated as

$$(t; x) = \sum_j \text{Res}(e^{st} \hat{\psi}(s; x); s_j) + \frac{1}{2\pi i} \int_{\Gamma} e^{st} \hat{\psi}(s; x) ds \quad (27)$$

where the first term is the sum of residues at the singularities inside the completed contour. The second term represents contributions to the integral from arcs at ∞ , and along branch cuts. In the case of the spiked TDP there is no branch cut, and the arc at ∞ makes no contributions, so we are left only with the first term, a sum of oscillations at discrete frequencies s_j that correspond to singularities of $\hat{\psi}(s; x)$. From (23) and (24) we see that singularities in $\hat{\psi}(s; x)$ must either be singularities of the homogeneous solutions f_+ ; f_- or zeroes of the Wronskian. For any finite s we can find

homogeneous solutions f_+ and f_- of (21); therefore, singularities in the Green's function can occur only at zeros of $W(s)$, and the residues in (27) must be taken at these zeros. But the vanishing of $W(s)$ at s_j means that f_+ / f_- at s_j , and hence that s_j is a QN frequency [8].

If, as in the case of the STDP, the only contributions to (27) occur in the sum, then we are left with

$$(\hat{t}; x) = \sum_X \text{Res}(e^{st} \hat{^}(s; x); s_j); \quad (28)$$

where the sum is over QN frequencies.

We now assume that the zeros of $W(s)$ are all first order, so that

$$W(s) = \frac{dW}{ds} \Big|_{s=s_j} (s - s_j) + O[(s - s_j)^2]; \quad (29)$$

For $x > x_1$ (i.e., for x to the right of the region in which the Cauchy data have support) we have, from (24) that

$$G(s; x; x^0) = \frac{f_-(s_j; x^0) f_+(s_j; x)}{dW/ds|_{s_j} (s - s_j)} + O[(s - s_j)^0] \quad (30)$$

and hence, from (23), the residues of $\hat{^}$ at s_j is

$$\text{Res}(\hat{^}(s; x) = \frac{e^{s_j t} f_+(s_j; x)}{dW/ds|_{s_j}} \int_{x_2}^{x_1} J(s_j; x^0) f_-(s_j; x^0) dx^0; \quad (31)$$

Finally, the sum over the QN basis functions can be written

$$(\hat{t}; x) = \sum_X b^j u_j(\hat{t}; x); \quad (32)$$

where

$$u_j(\hat{t}; x) = f_+(s_j; x) e^{s_j t} \quad (33)$$

and

$$b^j = \frac{1}{dW/ds|_{s_j}} \int_{x_0}^{x_1} (-\dot{f}_0(x^0) + s_{j-0}(x^0) f_-(s_j; x^0)) dx^0; \quad (34)$$

The waveform at $x_{\text{obs}} > x_1$ is then given by (5) with

$$i!_j = s_j \quad a^j = b^j f_+(s_j; x_{\text{obs}}); \quad (35)$$

This prescription has been applied to the spiked TDP, and the sine wave Cauchy data, with our standard choice of parameter values, $x_0 = 1$, $x_1 = 10$. Notice that our choice $x_2 = 5$ in (19) satisfies the criterion in the convergence proof that the continuous, but nonsmooth, Cauchy data have support only for $x > x_0 - 2 = 3(x_1 - x_0) = 5$. For this potential and these Cauchy data, the functions $\dot{f}_0(x)$, $-\dot{f}_0(x)$ and $f_-(s_j; x)$ are trigonometric or exponential functions, so the integral in (34) is elementary. Once the QN frequencies, s_j , and the factors $dW/ds|_{s_j}$ have been computed (as described in Appendix I), the coefficients are easily evaluated. The figures below show the result of using these coefficients in sums of the form (5).

Figure 8 shows the computed result for time evolution of the Cauchy data in the case that $V = 1$. This is compared along with mode sums for an increasing number of terms, up to $N = 10,001$ terms. Figure 9 shows the same plots in the case that $V = 10^{-6}$. In order to avoid cluttering the picture, we do not plot the values of the mode sums when they are far from having converged. These figures illustrate the fact that the mode sum converge faster for a larger $-\dot{f}_0$ -function. Also, for the smaller $-\dot{f}_0$ -function, the mode sum converge more rapidly at later times, with convergence "sweeping down" from late to early times.

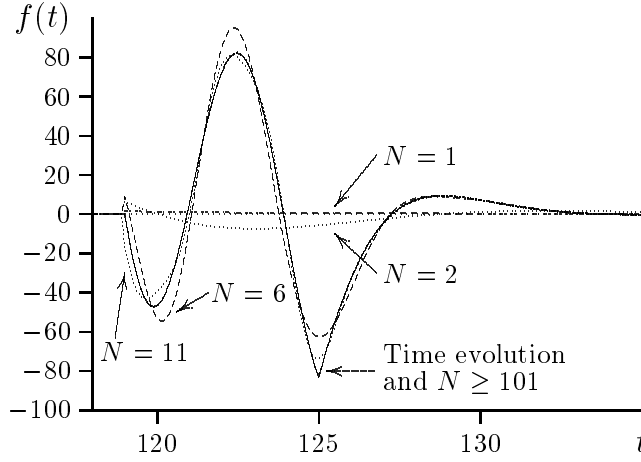


FIG. 8. Values of the mode sum for different number of terms N , compared to the wave form resulting from integrating the time dependent wave equation ($V = 1$).

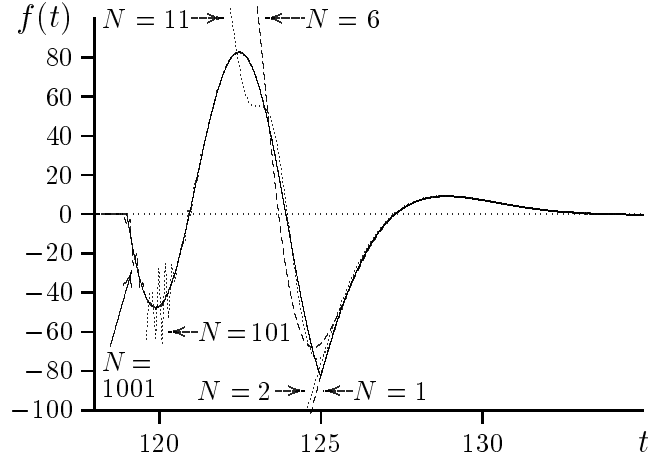


FIG. 9. Values of the mode sum for different number of terms N , compared to the wave form resulting from integrating the time dependent wave equation ($V = 10^{-6}$).

For a better view of the differences between the mode sums and the time evolved wave functions, Fig. 10 shows the logarithmic difference (evolved waveform vs. mode sum) for $V = 10^{-6}$.

Some of the systematics shown in these figures can be heuristically understood. The convergence in the $V = 1$ case is similar to that of a Fourier series (equally rapid at different times) since the QN frequencies, in this case, with small imaginary parts, are similar to the real frequencies of a Fourier series. On the other hand, for $V = 10^{-6}$, the damping of the additional (i.e., non-native) modes is much stronger and increases faster with N . Any error that originates from cutting off the mode sum after a finite number of terms can be regarded as being composed of modes with very strong damping; these modes are very large at early times.

We point out here an interesting technical feature of these results. The mode sums are so accurate at later times that the differences shown in Fig. 10 for $N = 10,001$, is actually dominated, after $t \approx 122$, by the numerical truncation error in computing the evolved waveform. A smaller time step in numerical evolution can improve the numerical accuracy of the computed waveform, and can move to a slightly larger time the point at which the evolution vs. sum difference is dominated by the numerical errors in the evolution.

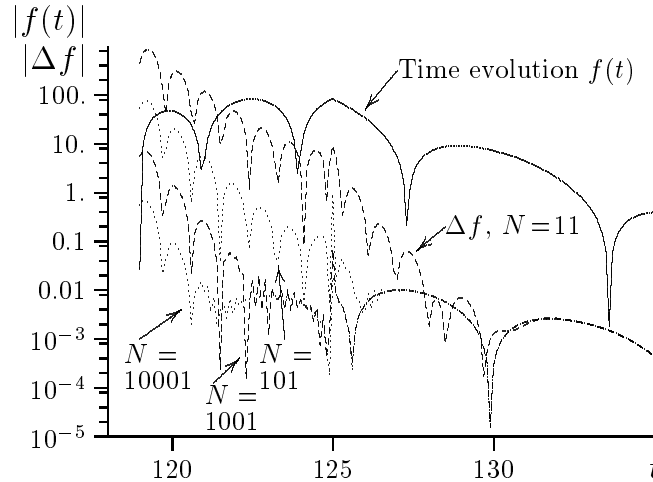


FIG. 10. Logarithmic difference between the values of the mode sum for different numbers of terms and the wave form resulting from integrating the time dependent wave equation ($V = 10^{-6}$).

IV. QUANTIFYING EXCITATION

A. The excitation coefficient

We now return to the question of how to quantify the excitation of QN oscillation. In Sec. II we defined the excitation coefficient A_k for a QN oscillation in a complete QN system. Due to the time shift problem, we argued that the excitation coefficient seems the only plausible indicator of the QN content of a waveform. In Sec. III we have seen that, at least in the particular example of the TDP, completeness can be induced in an incomplete system to create one that is "physically equivalent," i.e., differs negligibly in the evolution of Cauchy data. We can now ask whether, at least for the model problem at hand, we can use the excitation coefficients of the completed system to quantify the QN oscillation in the original ("native") system.

It is worth emphasizing that the TDP is a particularly simple starting point for these considerations, since it has only a single conjugate pair of native QN modes. The sine wave data we have used in the previous sections is also convenient since it produces a waveform (see Fig. 4) which clearly contains QN ringing, but contains significant oscillation at a different frequency ($\omega = 2\omega_0$).

The results of computations with this model are presented in Table I. Results are shown for the spiked TDP for different values of V and for the standard Cauchy data, a right moving sine wave initially extending over the interval $[5; 1]$. For comparison, a shifted sine wave, initially at $[8; 2]$, was also computed in the case $V = 10^{-6}$. Also included are results for the smooth TDP, and for the Zerilli equation with the Regge-Wehler potential with initial data corresponding to the Close Limit technique for black hole collisions [14].

The table presents values of excitation coefficients $A_1 = a_1^1(a_1) + (a_1^1)^*(a_1)$ and the energy excitation coefficients $E_1 = (\omega_1)^2(a_1) a_1^1 + (\omega_1^1)^2(a_1^*) a_1^*$, introduced in (13) and (15). In each case the QN frequency ω_1 is taken to be that eigenfrequency which corresponds to the native mode in the limit $V \rightarrow 0$; that is, ω_1 always lies on the path in the complex plane shown in Fig. 6. For small values of V this QN frequency is close to the native QN frequency ($\omega_1 + i = 2$). The waveform norm and the total energy are computed from waveforms obtained by explicit numerical integration of the wave equation (1). Also included are estimates for the numerical uncertainties of the results.

The norm and total energy can be computed from Eq. (9), or directly from the waveform. Similarly, the covariant coefficient may be computed from the contravariant ones, using Eq. (12), or from the waveform via Eq. (7). Even the contravariant coefficients can be obtained from the waveform itself, using an asymptotic t as it approaches a pure QN oscillation at the least damped QN frequency, instead of the residues of the Green's function through Eqs. (34) and (35). The waveform itself, in turn, can be obtained by direct numerical integration of the wave equation, or by using the mode sum as in Eq. (5). We have checked these alternatives for obtaining the quantities listed in the table; they result in essentially the same values as the route we have taken here.

We first notice that the values for the excitation coefficients are identical, within the numerical errors, for the original initial data (sine wave over the interval $[5; 1]$) and the shifted initial data (over the interval $[8; 2]$). This confirms our earlier argument that the excitation coefficients we have defined are independent of a translation of the initial data or, correspondingly, to a time shift of the evolved waveform.

$V(x)$	V	Initial data	A_1	E_1	f^2	\bar{f}^2
STDP	10^{-3}	Sine $[5; 1]$	40 854: 1:	23 810: 1:	19 246: 7:	27 404: 12:
STDP	10^{-6}	Sine $[5; 1]$	57 933: 1:	5 804:7 0:1	19 246: 7:	27 404: 12:
STDP	10^{-6}	Sine $[8; 2]$	57 934: 1:	5 804:5 0:3	19 246: 7:	27 404: 12:
STDP	10^{-7}	Sine $[5; 1]$	57 879: 1:	5 811:9 0:1		
STDP	10^{-8}	Sine $[5; 1]$	57 873: 1:	5 812:6 0:1		
STDP	10^{-9}	Sine $[5; 1]$	57 873: 1:	5 812:6 0:1		
TDP	{	Sine $[5; 1]$	57 872:8 ::	5 812:64 ::	19 248:0 ::	27 415:5 ::
Zerilli	{	Close Limit	10:699 10^{-4}		5:566 10^{-4}	

TABLE I. Excitation coefficients and norms for the spiked TDP QN system and for black holes in the close limit approximation.

It is important to realize that there are different ways to compute the quantities in the table, and several of them do not depend on the complete set of modes. The waveform and energy norm, of course, require only the waveform, but all coefficients can also be computed entirely from the waveform itself. The least damped QN frequency can be inferred from the asymptotic late time behavior, as can the contravariant coefficient for the least damped mode. [See (5).] Of the cases we study the least damped mode always corresponds to the native mode except for the $V = 1$ model. (See Fig.5.) Once the QN frequency is known the covariant coefficient can be computed directly from the integral in (7) and, with the contravariant coefficient known, the excitation and energy coefficients can then be found from (13) and (15). Since the quantities in the table can be computed from waveforms, we can compute them for the smooth TDP. In this case we do not have a complete set of modes, but that is irrelevant to the procedure for computation. (It turns out, in fact, that the simplicity of the smooth TDP and the sine wave data allows a closed form solution for the waveform, and for the norms and coefficients. This closed form solution has been used, and the values for the smooth TDP can be found for the table to essentially arbitrary precision.)

The numbers in the table make it clear that the results for the smooth TDP are the $V \rightarrow 0$ limit of the spiked TDP. This is obvious from a computational point of view, since all results can be computed from the waveform, and the $V \rightarrow 0$ waveform approaches the smooth TDP waveform. From another point of view, however, this result is interesting and important. It means that we can compute the excitation coefficient independent of the method with which completeness is induced. Put another way, it means that we can compute the excitation coefficient for a small completeness-inducing change, independent of the nature of the change. This conclusion, in fact, is crucial to the possible importance of the excitation coefficient. We could not use the excitation coefficient to characterize an excitation of a physical system if the value of the coefficient depended on our choice of a modification of that physical system.

The table also gives a value for the excitation coefficient for the gravitational radiation produced, in the close limit approximation [14], by the head on collision of two equal mass nonrotating holes. In this case the QN spectrum is infinite, but the QN oscillations are not complete. The excitation coefficient given is for the least damped of the QN oscillations, a frequency that appears to dominate the waveform produced.

Up to this point we have noted that computations with the model problem illustrate and confirm the features of the excitation coefficient that made it an attractive candidate for the quantification of the excitation of QN oscillations. Table I, however, also makes it unlikely that the excitation is a useful index of QN oscillation. For the small-spiked TDP the excitation coefficient is negative, and is larger (by a factor ~ 3) in magnitude than the norm. Note that we cannot ignore this "wrong" sign, and simply keep the large magnitude as an indication of a strong QN presence. Due to relation (9) we must conclude that the sum of all the other QN oscillations (those unrelated to the native QN mode) must be greater (by a factor ~ 4) than the norm. For the close limit waveform the excitation coefficient is roughly twice the size of the norm off and hence the sum of excitation coefficients of all other QN oscillations (if the system were made complete somehow) would be negative.

As a possible alternative to the excitation coefficient we have also computed the energy excitation coefficient, as defined in (15). The results listed for E_1 and the norm of f , however, do not make this any more attractive as a measure of QN excitation.

At this point, we also note that the excitation coefficient A_1 is not related to the norm of the QN mode contribution corresponding to the first pair of modes, i.e. of $b^1 u_1 + (b^1 u_1)^*$. Similarly, the energy excitation coefficient E_1 is no measure for the energy of this QN mode contribution.

It is, of course, impossible to prove that something like quantifying QN excitations cannot be done in a mathematically acceptable way. Despite this, and perhaps to provoke further work (by others!) we are tempted to offer the following very tentative conclusion: Consider the following three conditions, which allow a mathematically meaningful as well as a useful measure of excitation; they are all satisfied for normal mode systems:

The measure of excitation is independent of a simple shift of the waveform (i.e. a shift in space of the initial data, corresponding to a shift in time for the time evolved waveform).

Excitation strength can be quantified individually for any number of modes, with the individual excitations adding up to the total norm of the waveform.

The measure of excitation is useful for quantifying the excitation in a comparative way; in particular, it always lies between 0% and 100%.

We conjecture: There is no quantification of QN oscillations of the waveform, based on the algebra of the function space of QN oscillations, which satisfies all three of these criteria.

The excitation coefficients we are defining in this paper satisfy the first two conditions, but not the third one (In Table I we see that the excitation coefficient can be negative and can be greater than 100%.) One might regard these two conditions as related to mathematical properties of the QN mode system, while the third one is of a more practical

significance. We are currently investigating another technique to quantify excitations, with a measure that satisfies the first and third criteria, but not the second one. This measure may turn out to be of some practical utility, but is not as closely related to the mathematics of the function space as are the present considerations. A description of this work will be published elsewhere.

Our conjecture is based specifically on the appearance of the excitation coefficient as the only quantity in that function space that solves the "time shift" problem, and on the observed failure of the excitation coefficient to be "useful." It is also based, less specifically, on our belief that there are differences between normal mode and QN systems that cannot be bridged. For this reason we speculate that inducing completeness, while it is mathematically interesting, is not likely to lead to useful tools for understanding the underlying native system. The reason is that the spectrum of added QN frequencies is unrelated to the native system and characterizes only the method used to induce the completeness. We, in fact, are willing to extrapolate in the direction of this speculation. We conjecture that in a complete QN spectrum which has a dense set of frequencies, and a small number of "isolated" frequencies, like the spectrum of the spiked TDPs in Fig. 5, it is useful to modify the system to remove completeness, in order to get a more useful understanding and a simplified method of analysis. The obvious example of this is removing the functions from the spiked TDP problem in order to get a physically equivalent, but simpler incomplete system.

A very similar point of view is that in a QN spectrum, not all frequencies are equally important. Some will actually be evident in waveforms produced in the evolution of generic Cauchy data; others won't. For the small spectra of Fig. 5, the "interesting" QN frequencies are the isolated ones near $(1+i)=2$. In the $V = 1$ case, on the other hand, there is again the appearance of QN ringing in the waveform, but the spectrum contains no isolated frequency. A similar situation was found in a study where the Regge-Wheeler potential was replaced by a series of step potentials [13]. More generally, one should ask: If one has only the spectrum and the associated quantities (e.g., the metric matrix), is there a way of identifying which QN frequencies are "important" in the sense of really characterizing the evolution of Cauchy data? In this sense we are asking a question related to "to what extent are (some) QN modes like normal modes?" since normal modes do characterize the system in which they arise.

B. Condition number of the metric matrix

The metric matrix (11) would appear to be a likely place to find a way of characterizing a QN system without regard to specific waveforms produced by specific Cauchy data. We will now discuss some numerical results which confirm the intuitive insight we had gained by doing thought experiments on specific Cauchy data in Sec. IID. Studying the metric matrix directly, we don't need to refer to specific initial data any more, as we had to do before.

We first note the singular nature of the infinite metric matrix in two cases. To characterize this singular property we truncate the set of QN functions, keeping only the first D . We then compute the condition number R (ratio of maximum to minimum eigenvalue) for the D -dimensional subspace. The condition number as a function of D_{sub} is plotted in

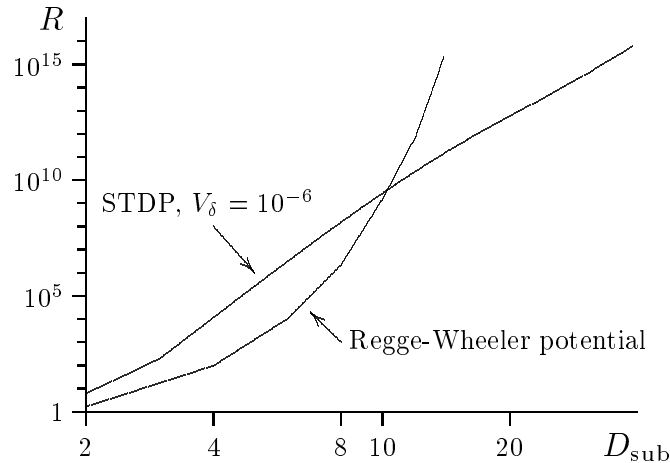


FIG. 11. The condition number R for the metric matrix for a truncated subspace of dimension D_{sub} , spanned by the first D_{sub} QN basis functions. Results are shown for both the spiked TDP ($V = 10^{-6}$) and the Regge-Wheeler potential.

Fig. 11 for two cases: the spiked TDP and the QN spectrum of Schwarzschild black holes (the QN modes of the Zerilli

or Regge-Wheeler potentials). For the spiked TDP the approximately straight line in the log-log plot suggests that the condition number increases roughly as the twelfth power of the dimension D_{sub} of the subspace. For the black hole QN spectrum the increase is even more dramatic, suggesting perhaps a "more singular" metric for this incomplete QN spectrum.

C. Angles between basis functions

In Sec. II we introduced covariant basis functions $\phi_n(t)$ with the definition $\phi_n(t) = e^{i\omega_n t}$. If the basis functions $e^{i\omega_n t}$ were orthogonal we would have that $\phi_n(t)$ and $e^{i\omega_n t}$ are "parallel," that is, $\phi_n(t) \propto e^{i\omega_n t}$. It is plausible that such statements as "this wave is dominated by oscillation at the fundamental QN frequency" are most meaningful if the covariant and contravariant basis vectors are nearly "parallel." To measure the extent to which $\phi_j(t)$ and $e^{i\omega_j t}$ fail to be proportional we can introduce an angle θ_j between them, defined by

$$\cos(\theta_j) = \frac{\langle \phi_j(t) | e^{i\omega_j t} \rangle}{\|\phi_j(t)\| \|e^{i\omega_j t}\|} = \frac{1}{\sqrt{G_{jj} G^{jj}}}; \quad (36)$$

where G^{ij} is the matrix inverse of G_{ij} .

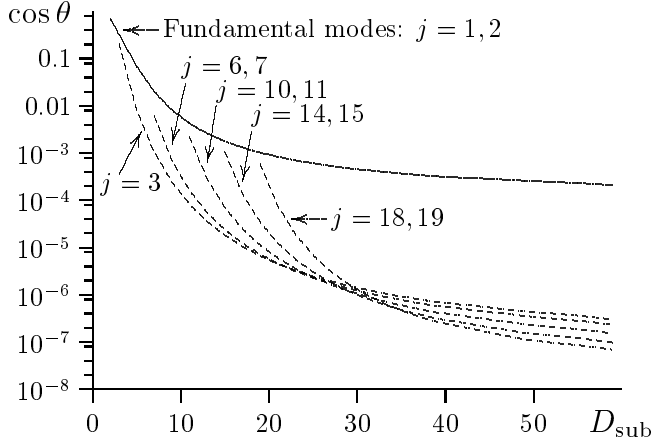


FIG. 12. Cosine of angles between several contravariant and covariant basis vectors, as a function of the dimension of a subspace spanned by D_{sub} QN modes of the spiked TDP with $V = 10^{-6}$.

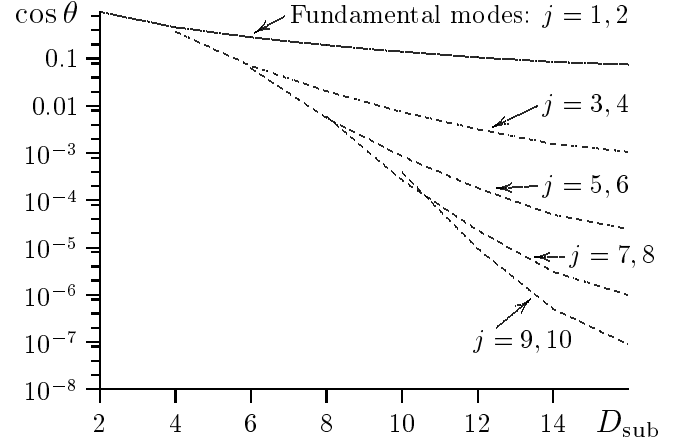


FIG. 13. Cosine of angles between several contravariant and covariant basis vectors, as a function of the dimension of a subspace spanned by D_{sub} QN modes of the Regge-Wheeler potential.

The components of the infinite matrix G^{ij} cannot be computed, so again we truncate a subspace by keeping only the first D_{sub} vectors, and we compute the angles in that subspace with (36). Results are shown in Fig. 12 for the spiked TDP with $V = 10^{-6}$. The value of $\cos(\theta_j)$ is shown for several QN modes as a function of D_{sub} , the dimension at which the subspace is truncated. Figure 13 shows $\cos(\theta_j)$ for the black hole QN spectrum. In Fig. 12, the decrease of $\cos(\theta_1)$, corresponding to the native mode, is much slower than that of the additional modes. One might speculate that this is related to the fact that the native mode is more characteristic of the system than the additional ones. No such clear distinction can be seen in Fig. 13 for the case of the Regge-Wheeler potential. However, the angles increase much faster for the more highly damped modes as well, which might again indicate that the fundamental, least damped mode is more characteristic of the system than the more strongly damped ones.

V. ACKNOWLEDGMENTS

We wish to thank Ted Newman for useful discussions and numerous helpful suggestions on the presentations of these results. We also thank Karel Kuchar, Wai-Mo Suen, and John Wheeler for useful discussions during the development of this work. We thank the Deutsche Forschungsgemeinschaft for support through SFB 382 and NATO for support through grant CRG 971092. One of us (RHP) thanks the National Science Foundation for support under grants PHY 95-07719 and PHY 97-34871.

APPENDIX I. FINDING QUASINORMAL FREQUENCIES OF THE TDP AND OF THE SPIKED TDP

A. The unmodified TDP

The TDP is defined as

$$V(x) = \begin{cases} 0 & x < x_0 \\ \frac{1}{l(l+1)}x^2 & x \geq x_0 \end{cases}; \quad (37)$$

where l is an integer. We look only at $l=1$, but the procedure can easily be extended for larger values of l . Also, we will generally let $x_0 = 1$.

The domain of the wave equation is naturally divided into two regions:

I. $x < x_0$ In this region, the potential vanishes, and therefore the wave equation has the two trivial solutions:

$$\psi_1(x) = e^{+i!x} \quad (38)$$

$$\psi_2(x) = e^{-i!x} \quad (39)$$

II. $x \geq x_0$ For integer values of l , the solutions are given by finite sums. For $l=1$, we have

$$\psi_{11}(x) = e^{+i!x} \left(1 + \frac{1}{i!x} \right) \quad (40)$$

$$\psi_{12}(x) = e^{-i!x} \left(1 + \frac{1}{i!x} \right); \quad (41)$$

Obviously, the solutions satisfying the required boundary conditions at negative and positive infinity are

$$\psi_-(x) = \psi_1(x) \quad (x < x_0) \quad (42)$$

$$\psi_+(x) = \psi_{12}(x) \quad (x \geq x_0); \quad (43)$$

In general, of course, $\psi_-(x)$ will be a linear combination of $\psi_{11}(x)$ and $\psi_{12}(x)$ for $x \geq x_0$, and $\psi_+(x)$ a combination of $\psi_1(x)$ and $\psi_2(x)$ for $x < x_0$. A quasinormal mode is a solution where both boundary conditions are satisfied simultaneously, i.e. $\psi_-(x) = \psi_+(x)$. The easiest way to find out if this is the case is to compare $\psi_-(x)$ and $\psi_+(x)$, as defined in (42), at $x = x_0$. Strictly speaking, $\psi_-(x)$ is not defined at $x = x_0$. However, any solution of the wave equation will have to be continuous, and have a continuous first derivative, at $x = x_0$. It is therefore permissible to use the left limit of $\psi_-(x)$ and of $\psi_+'(x)$ as $x \rightarrow x_0^-$, and compare them with the values of $\psi_+(x)$ and $\psi_+'(x)$ at $x = x_0$.

The comparison is done using the Wronskian determinant of $\psi_-(x)$ and $\psi_+(x)$:

$$\begin{aligned} W[\psi_-; \psi_+](x_0) &= \psi_-(x_0) \psi_+'(x_0) - \psi_-'(x_0) \psi_+(x_0) \\ &= 2i! \left(\frac{2}{x_0} - \frac{1}{i!x_0^2} \right) \end{aligned} \quad (44)$$

Solving the equation $W[\psi_-; \psi_+](x_0) = 0$ for $!$ yields the quasinormal frequencies

$$! = \frac{1+i}{2x_0} \quad (45)$$

Therefore, for $l=1$, there is only one pair of quasinormal frequencies.

B. QN frequencies of the spiked TDP

We define the 'spiked' potential as

$$\bar{V}(x) = V(x) + V(x - x_0); \quad (46)$$

We now have to distinguish three areas:

I. $x < x_0$ This region is identical to region I for the unmodified potential, with the same set of two solutions.

IIa. $x_0 < x < x_1$ Again, there are two linearly independent solutions

$$\Psi_{IIa1}(x) = e^{+iLx} \left(1 - \frac{1}{iLx}\right) \quad (47)$$

$$\Psi_{IIa2}(x) = e^{-iLx} \left(1 + \frac{1}{iLx}\right) : \quad (48)$$

IIb. $x > x_1$ The two linearly independent solutions are

$$\Psi_{IIb1}(x) = e^{+iLx} \left(1 - \frac{1}{iLx}\right) \quad (49)$$

$$\Psi_{IIb2}(x) = e^{-iLx} \left(1 + \frac{1}{iLx}\right) : \quad (50)$$

In our notation the function $\Psi_{IIb2}(x)$, for example, refers to the solution in all regions that, in region IIb, has the functional form shown in Eq. 50.

Due to the function separating regions IIa and IIb, the solutions $\Psi_{IIa2}(x)$ and $\Psi_{IIb2}(x)$ are not the same. Rather, $\Psi_{IIb2}(x)$ will be a linear combination of $\Psi_{IIa1}(x)$ and $\Psi_{IIa2}(x)$ in region IIa:

$$\Psi_{IIb2}(x) = p_1 \Psi_{IIa1}(x) + p_2 \Psi_{IIa2}(x) \quad (51)$$

Once again, the solutions

$$\Psi(x) = \Psi_I(x) \quad (x < x_0) \quad (52)$$

$$+ \Psi_{IIb2}(x) \quad (x > x_1) \quad (53)$$

satisfy the boundary conditions at negative and positive infinity. However, in order to compare solutions at $x = x_0$, we now have to determine the representation of $\Psi_{IIb2}(x)$ in region IIa, i.e. we need to know the coefficients for the linear combination (51).

These coefficients can be determined using the junction conditions for any solution $\Psi(x)$ of the wave equation across the function:

1. $\Psi(x)$ must be continuous at x
2. the derivative $\Psi'(x)$ must have a discontinuity given by

$$\Psi'(x^+) - \Psi'(x^-) = V \Psi(x) \quad (54)$$

The second condition is obtained by integrating the wave equation from $x = x_0 - \epsilon$ to $x = x_0 + \epsilon$, letting $\epsilon \rightarrow 0$ and using the first condition.

Using Ψ_{IIb2} for $\Psi(x^+)$ and Eq. (51) for $\Psi(x^-)$, we can solve these conditions for p_1 and p_2 . We obtain

$$p_1 = V \frac{[\Psi_{IIa2}(x)]^2}{W_{+12}} \quad (55)$$

$$p_2 = 1 - V \frac{\Psi_{IIa1}(x) \Psi_{IIa2}(x)}{W_{+12}} \quad (56)$$

where $W_{+12} = W[\Psi_{IIa1}; \Psi_{IIa2}] = 2iL$.

Therefore,

$$\begin{aligned} W[\Psi_I; \Psi_{IIb2}](x_0) &= W[\Psi_I; \Psi_{IIb2}](x_0) = p_1 W[\Psi_I; \Psi_{IIa1}](x_0) + p_2 W[\Psi_I; \Psi_{IIa2}](x_0) \\ &= R_1 + V [R_2 + R_3 e^{2iLx_0}] \end{aligned} \quad (57)$$

where $L = x_0 - x_1$, and $W[\Psi_I; \Psi_{IIa1}](x_0) = e^{2iLx_0} = (iLx_0^2)$, and thus

$$R_1 = W[\pi; \pi_{a2}](x_0) = 2i! \frac{2}{x_0} \frac{1}{i! x_0^2} \quad (58)$$

$$R_2 = \frac{\pi_{a1}(x) \pi_{a2}(x)}{W + 12} W[\pi; \pi_{a2}](x_0) = 1 \frac{1}{(i! x)^2} \left(1 + \frac{1}{i! x_0} + \frac{1}{2(i! x_0)^2} \right) \quad (59)$$

$$R_3 = e^{2i!L} \frac{\pi_{a2}(x)^2}{W + 12} W[\pi; \pi_{a1}](x_0) = \frac{1}{2(i! x_0)^2} \left(1 + \frac{1}{i! x} \right)^2 \quad (60)$$

The quasinormal frequencies of the spiked TDP can now be computed numerically by searching for roots of the equation

$$W[\pi; \pi_a](x_0) = 0 \quad (61)$$

C. Asymptotic approximation for the QN frequencies of the spiked TDP

It is possible to find an asymptotic formula for the QN frequencies under the assumption that the absolute value of the frequency becomes large. We start by assuming that in (61), we have $j! x_0 j \gg 1$ and $j! x \gg 1$. The condition for QN frequencies can then be written

$$2i! x_0 + O([!x]^0) + V \left(1 + O([!x]^{-1}) \right) + \frac{e^{2i!L}}{2(i! x_0)^2} \left(1 + O([!x]^{-1}) \right) = 0 \quad (62)$$

where x is the minimum of x_0 and x . It is clear that for $j! x j \gg 1$ there can be solutions only if

$$2i! + V \frac{1}{2(i! x_0)^2} e^{2i!L} = 0 \quad (63)$$

and we use this approximation to find an iterative solution for the QN frequencies. We start by taking the cube root of

$$e^{2i!L} = \frac{4(i!)^3 x_0^2}{V} \quad (64)$$

to write

$$e^{\frac{2}{3}i!_R L} e^{\frac{2}{3}i!_I L} e^i = \frac{4x_0^2}{V} i! \quad A i! \quad (65)$$

where $= j \frac{2}{3}$; $j = 0; 1; 2$.

Taking the absolute values on both sides gives

$$e^{\frac{2}{3}i!_I L} = A j! j \quad (66)$$

With $i!_R + i!_I$ this last relation already shows that $i!_I = j! j$ is required for a QN frequency.

Using (66) to rewrite (65) we find

$$\cos\left(\frac{2}{3}L i!_R + \right) - i \sin\left(\frac{2}{3}L i!_R + \right) = i \frac{i!}{j! j} \quad (67)$$

We now make the approximation $i!_I = 0$, i.e. $i!_R = j! j$ leading to

$$\cos\left(\frac{2}{3}L i!_R + \right) = 0; \quad \sin\left(\frac{2}{3}L i!_R + \right) = 1 \quad (68)$$

$$\frac{2}{3}L i!_R = \frac{\pi}{2} + 2N \quad \frac{2}{3}j \quad ; \quad N = 0; 1; \dots; j = 0; 1; 2 \quad (69)$$

or equivalently

$$(\mathbf{!}_R)_n = \frac{1}{L} \left(\frac{3}{4} + n \right); \quad n = 0; 1; \dots \quad (70)$$

An approximation for $\mathbf{!}_I$ is then obtained by using (66):

$$(\mathbf{!}_I)_n = \frac{3}{2L} (\ln A + \ln \mathbf{!}_R) \quad (71)$$

The approximate solutions of (70) and (71) can now be iteratively improved. We rewrite (61) as

$$e^{2i\mathbf{!}_I L} = \frac{R_1 + V R_2}{V R_3} = :R(\mathbf{!}) = R(\mathbf{!}_R; \mathbf{!}_I) \quad (72)$$

and take absolute values to get

$$e^{2\mathbf{!}_I L} = \mathfrak{R} j \quad (73)$$

$$\mathbf{!}_I = \frac{\ln \mathfrak{R} j}{2L} \quad (74)$$

With these inserted in (72) we arrive at

$$\cos(2\mathbf{!}_R L) = \frac{\langle R \rangle}{\mathfrak{R} j}; \quad \sin(2\mathbf{!}_R L) = \frac{= (R)}{\mathfrak{R} j} : \quad (75)$$

This can be used as an iterative method to find the p^{th} iteration from the $p-1^{\text{th}}$ approximation, as follows:

$$\cos(2(\mathbf{!}_R)^p L) = \frac{\langle R((\mathbf{!}_R)^{p-1}; (\mathbf{!}_I)^{p-1}) \rangle}{\mathfrak{R}((\mathbf{!}_R)^{p-1}; (\mathbf{!}_I)^{p-1}) j}; \quad \sin(2(\mathbf{!}_R)^p L) = \frac{= (R(\dots))}{\mathfrak{R}(\dots) j} \quad (76)$$

and

$$(\mathbf{!}_I)^p = \frac{\ln \mathfrak{R}((\mathbf{!}_R)^p; (\mathbf{!}_I)^{p-1}) j}{2L} \quad (77)$$

This iterative solution can be started with any value of n in the zeroth approximation of (70) and (71), and the iteration converges to the exact solution. The iteration cannot be used to find the native QN frequency of the smooth TDP since $V = 0$ in that case.

APPENDIX II. PROOF OF CONVERGENCE

A proof is given here of the convergence of the sum of quasinormal excitations for the spiked TDP under appropriate restrictions on the Cauchy data. To do this we start by defining the integral

$$I(d_1) = \int_{-\infty}^{\infty} F(s) ds = \frac{1}{2-i} \int_{-\infty}^{\infty} \frac{s^2 (s) e^{s(d_1+d_2)}}{(s)} ds : \quad (78)$$

Here (s) is defined to be

$$(s) = P_1(s) + e^{2sL} s^3 P_2(s); \quad (79)$$

in which P_1 and P_2 are polynomials of finite order in $1=s$:

$$P_1(s) = A_1 + B_1 s + \dots + A_2 + B_2 s + \dots : \quad (80)$$

The path of integration in the complex s plane is along the vertical axis, from $-iL$ to $+iL$. For $\langle s \rangle = 0$ the function (s) is required to have the property that for some real constants K and p

$$|j(s)j| < \frac{K}{\mathfrak{R} j} : \quad (81)$$

(This condition will be related below to restrictions on acceptable Cauchy data.) The constants appearing in (78) are taken to satisfy the following conditions: (i) The ratio A_1/A_2 is real and positive. (ii) $L; d_1$ and d_2 are real and nonnegative, and $2L > d_2$. (iii) The constant p appearing in (81) must be large enough that

$$p + \frac{3d_2}{2L} > 0 : \quad (82)$$

The roots of are denoted s_k . (They represent, of course, the QN frequencies according to the usual correspondence $s \leftrightarrow i\omega$.) Since they must occur in complex conjugate pairs it is convenient here to use the notation $s_1; s_{-1}; s_2; s_{-2};$ with s_k indicating the corresponding roots with positive and negative imaginary parts.

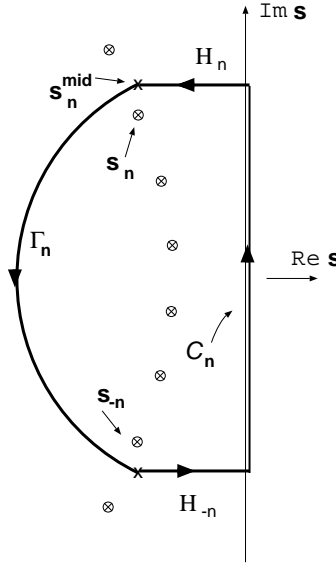


FIG. 14. Contour for proving convergence for the spiked TDP oscillations.

What we will prove is that under the conditions stated above $I(d_1)$ can be written as

$$I(d_1) = \sum_{k=-1}^{k=N+1} a^{(k)} e^{s_k d_1} \quad (83)$$

where

$$a^{(k)} = \oint_{\Gamma} (s_k) e^{s_k d_2} = (d_2 - ds) \int_{s=s_k} : \quad (84)$$

The convergence of the sum in (83) is not uniform at $d_1 \rightarrow 0$, but is uniform for any interval of d_1 bounded away from 0. We give the details of the relationship to the physical problem of Sec. III after we prove the main result above. The proof is organized with a set of lemmas.

Lemma 1: Let $s_n^{\text{mid}} = s_n + i\pi/2L$ and let H_n be the horizontal path (as shown in Fig. 14) in the s plane from the imaginary s axis to the point s_n^{mid} . Let

$$I_{H_n} = \int_{H_n}^Z F(s) ds \quad (85)$$

be the integral of $F(s)$ on this path, then N can be chosen so that for $n > N$

$$|I_{H_n}| \leq \text{const} \cdot n^{-p} \quad (3d_2 = 2L) : \quad (86)$$

Proof: The discussion of the roots of the spiked TDP Wronskian in Appendix I can be applied to the roots of . For large n , the n dependence of the roots takes the form

$$\text{Re}(s_n) = n\pi/2L + \text{const} : + \quad (87)$$

$$\text{Im}(s_n) = (3\pi/2L) \ln(n) + \text{const} : + \quad (88)$$

It follows that a constant can be chosen so that $\beta_n j > \text{const}$ on H_n , and hence $j(s) < 2K = n^p$, for some constant K independent of n . Since $\langle(s) = 0$ on H_n and d_1 is nonnegative, we have that $\beta^{sd_1} j \leq 1$. With $s = s_n + i = 2L + i$ and with i running from $\langle(s_n)$ to 0 on the path H_n , the integral must satisfy

$$|\mathcal{I}_{H_n} j| \leq \frac{K}{n^{p-2}} \int_0^{\langle(s_n)} \frac{d}{D(s)} ; \quad (89)$$

where $D(s) = e^{sd_2} \langle(s)$. On H_n we have that

$$e^{2Ls} = e^{2Ls_n} e^{2Li} \quad (90)$$

and $D(s)$ can be written as

$$D(s) = P_1(s_n) e^{i \langle(s) d_2} e^{\langle(s) d_2} R_1 + e^{2Li} e^{\langle(s) d_2} R_2 \quad (91)$$

where

$$R_1 = \frac{P_1(s)}{P_1(s_n)} \quad R_2 = \frac{s^3 P_2(s)}{s_n^3 P_2(s_n)} ; \quad (92)$$

For n larger than some N we can make both R_1 and R_2 arbitrarily close to unity. For $n > N$ it follows that the magnitude of the sum in square brackets in (91) must be larger than the second term, and hence

$$|\mathcal{I}(s)j| > |P_1(s_n)| e^{2Li} e^{\langle(s) d_2} |R_2 j| \quad (93)$$

By choosing N large enough we can make $|P_1(s_n)j|$ and $|R_2 j|$ larger than n -independent constants, so that

$$|\mathcal{I}(s)j| > \text{const} \cdot e^{2Li} e^{\langle(s) d_2} = \text{const} \cdot e^{2Li} e^{\langle(s_n) d_2} e^{-d_2 i} ; \quad (94)$$

We have then that

$$\begin{aligned} |\mathcal{I}_{H_n} j| &\leq \frac{K}{n^{p-2}} e^{\langle(s_n) d_2} \int_0^{\langle(s_n)} e^{(d_2 - 2L)i} di \\ &< \frac{K}{n^{p-2}} e^{\langle(s_n) d_2} \frac{1}{2L - d_2} ; \end{aligned} \quad (95)$$

It follows from (87) that we can choose a constant so that $\beta^{\langle(s_n) d_2} j < \text{const} = n^{(3d_2=2L)}$, and therefore that

$$|\mathcal{I}_{H_n} j| \leq \frac{\text{const}}{n^{p+(3d_2=2L)-2}} ; \quad (96)$$

which was to be proven. A similar proof shows that the same result applies to $\mathcal{I}_{H_n} j$.

Lemma 2: On the arc γ_n from $s_n^{m \text{ id}}$ to $s_n^{m \text{ id}}$ with $\beta j = \beta_n^{m \text{ id}} j$, the magnitude of $\langle(s)$ is larger than some constant that is independent of n .

Proof: We write

$$\langle(s) = P_1(s) [1 + \langle(s)] \quad (97)$$

where

$$\langle(s) = e^{2sL} s^3 P_2(s) = P_1(s) ; \quad (98)$$

We must show that $|1 + \langle(s)|$ is bounded from below by an n -independent constant. We recall that $s_n^{m \text{ id}} = s_n + i = 2L + i$ and that $\langle(s_n) = 1$, so that

$$\langle(s_n^{m \text{ id}}) = \frac{s_n^{m \text{ id}}}{s_n} \frac{s_n^3 P_2(s_n^{m \text{ id}})}{P_2(s_n)} \frac{P_1(s_n)}{P_1(s_n^{m \text{ id}})} ; \quad (99)$$

For n larger than some N_{min} we have that $\langle(s_n^{m \text{ id}})$ is arbitrarily close to unity, so that

$$(s_n^{m \text{ id}}) = 1 + \quad ; \quad (100)$$

and $N_{m \text{ in}}$ can be chosen large enough to make j arbitrarily small.

On the arc γ_n we write (s) as

$$(s) = e^{2sL} s^3 (A_2 = A_1) [1 + (s)] : \quad (101)$$

By choosing $N_{m \text{ in}}$ sufficiently large, we can bound the magnitude of (s) to be less than an arbitrarily small n -independent constant. For s on the arc γ_n , we now write s as

$$s = R_n i e^{i\theta_n} ; \quad (102)$$

where $R_n = j_n^{m \text{ id}}$ and θ_n is the counterclockwise angle from the positive imaginary s axis to the point s on γ_n . We denote by ϕ_n the angle to $s_n^{m \text{ id}}$, so that $s_n^{m \text{ id}} = R_n i e^{i\phi_n}$ and we write $\theta_n = \phi_n + \psi_n$. In terms of this notation we have

$$(s) = F_0 F_1(\psi_n) F_2(\psi_n) ; \quad (103)$$

where

$$F_0 = (1 + \psi_n)(1 + (s)) = (1 + (s_n^{m \text{ id}})) \quad (104)$$

$$F_1 = e^{2iL R_n [\cos(\phi_n + \psi_n) - \cos(\phi_n)]} e^{3i\psi_n} \quad (105)$$

$$F_2 = e^{2L R_n [\sin(\phi_n + \psi_n) - \sin(\phi_n)]} ; \quad (106)$$

The complex phase of (s) is near zero at $s = s_n^{m \text{ id}}$, and decreases as s moves counterclockwise along the arc γ_n . We use the expressions above to find at what value of ψ_n the phase of (s) first becomes $\pi/2$. We note that $j_n = 1$ and on the top half of the arc $F_2 = 1$. The value of ψ_n is given by

$$2L R_n [\cos(\phi_n + \psi_n) - \cos(\phi_n)] + 3\psi_n + (\phi_n + \psi_n) = \pi/2 ; \quad (107)$$

where ϕ_n is the phase of F_0 . We note that

$$j \cos(\phi_n + \psi_n) - \cos(\phi_n) > \sin(\phi_n) : \quad (108)$$

From (87) we know that $\sin \phi_n$ decreases with n as $\ln(n) = n$, and R_n increases as n . Thus the first term in (107) is larger than the second by a factor that increases as $\ln(n)$. The third term, the ψ_n term, decreases with increasing n , and we can bound it to be smaller than an arbitrarily small constant by choosing $N_{m \text{ in}}$ sufficiently large. From these considerations it follows that we can choose $N_{m \text{ in}}$ large enough that the magnitude of the first term in (107) is larger than, say, $2/3$ of the magnitude of the left hand side, and hence satisfies

$$2L R_n [\cos(\phi_n) - \cos(\phi_n + \psi_n)] > \pi/3 : \quad (109)$$

Let us also take $N_{m \text{ in}}$ large enough so that $\phi_n + \psi_n < \pi/4$. In that case we have

$$\frac{\sin(\phi_n + \psi_n) - \sin(\phi_n)}{\cos(\phi_n) - \cos(\phi_n + \psi_n)} > 1 : \quad (110)$$

From this it follows that $2L R_n [\sin(\phi_n + \psi_n) - \sin(\phi_n)] > \pi/3$, and hence $F_2 < e^{-\pi/3}$. Since the deviation of $F_0 j$ from unity is arbitrarily small, let us use $F_0 j < e^{-\pi/2}$ and conclude that $j < e^{-\pi/4}$ at the point along γ_n at which (s) first becomes purely imaginary. As ψ_n increases, the magnitude of (s) continues to decrease. It follows that for every point along the top of the arc

$$j + j > 1 - e^{-\pi/4} : \quad (111)$$

A similar analysis starting at s_n shows that (110) holds also for the bottom half of the arc.

Lemma 3: On the arc γ_n from $s_n^{m \text{ id}}$ to $s_n^{m \text{ id}}$ with $j = j_n^{m \text{ id}}$, the integral

$$I_n(d_1) = \frac{1}{2} \int_{-i}^Z \frac{s^2 (s) e^{s(d_1 + d_2)}}{(s)} ds \quad (112)$$

satisfies,

$$J_n(d_1) \leq \frac{\text{const}}{n^{p+(3d_2=2L)-2}}; \quad (112)$$

where the constant is independent of n .

Proof: On γ_n we have that $\text{Re}(s) \leq \text{Re}(s_n)$, so that

$$e^{sd_2} \leq e^{\text{Re}(s_n)d_2} \quad (113)$$

and, for some constant, the right hand side of (113) is less than $\text{const} \cdot n^{(3d_2=2L)}$. We have seen that J_n is bounded from below on γ_n . With the bound on $J_n(s)$ from (81), we have then that

$$J_n(d_1) \leq \frac{\text{const}}{n^{p+(3d_2=2L)-2}} \int_n e^{\text{Re}(s)d_1} |J_n(s)| ds; \quad (114)$$

Since the integrand is everywhere nonnegative, we have that

$$\int_n e^{\text{Re}(s)d_1} |J_n(s)| ds \leq \int_{\text{arc}} e^{\text{Re}(s)d_1} |J_n(s)| ds; \quad (115)$$

where the arc is the half circle with $|s| = R_n$ in the left half plane. But, the integral along the half circle is

$$\begin{aligned} \int_{\text{arc}} e^{\text{Re}(s)d_1} |J_n(s)| ds &= R_n \int_0^\pi e^{-d_1 R_n \sin \theta} d\theta = 2R_n \int_0^{\pi/2} e^{-d_1 R_n \sin \theta} d\theta \\ &\leq R_n \int_0^{\pi/2} e^{-2d_1 R_n \sin \theta} d\theta = \frac{1}{d_1} (1 - e^{-d_1 R_n}) \end{aligned} \quad (116)$$

This completes the proof of the lemma.

Proof of main result: We define C_n as the integration path on the imaginary s axis from $i = (s_n) - i = 2L$ to $i = (s_n) + i = 2L$, and we define

$$I_n(d_1) = \int_{C_n} F(s) ds; \quad (117)$$

We let $I_{n,\text{closed}}(d_1)$ be the integral on the closed path consisting of C_n , of γ_n , of H_n and of \bar{H}_n traced backwards. From the lemma above we have

$$J_n(d_1) - I_{n,\text{closed}}(d_1) \leq J_n(d_1) + J_{H_n}(d_1) + J_{\bar{H}_n}(d_1) \leq \frac{\text{const}}{n^{p+(3d_2=2L)-2}}; \quad (118)$$

The integral on the closed path is $2\pi i$ times the sum of the residues inside the path,

$$I_{n,\text{closed}}(d_1) = \sum_n^{X^n} a^{(k)} e^{s_k d_1}; \quad (119)$$

where $a^{(k)}$ is the residue of $s^2 F(s) e^{sd_2}$ at $s = s_k$. Since the only singularities of the integrand in the finite s plane are simple poles at the roots of $F(s)$, these $a^{(k)}$ coefficients are those defined in (84). We have then

$$J_n(d_1) - \sum_n^{X^n} a^{(k)} e^{s_k d_1} \leq \frac{\text{const}}{n^{p+(3d_2=2L)-2}} \quad (120)$$

and our main result follows from the fact that $I(d_1)$ is the limit of $I_n(d_1)$ as $n \rightarrow \infty$.

We now turn to the role played by the Cauchy data. In the Green function solution for the waveform [see the discussion following (21)], a function of s appears representing the integral of the product of $f(s; x)$ and the combination $J(x; s) \rightarrow \phi(x) = \phi_0(x)$. In the case of the TDP or spiked TDP, $f(s; x) = e^{sx}$. Let us suppose that the support of the Cauchy data is confined to the region $x_2 < x < x_1$. The Cauchy data then enters the s integral through the function

$$J(s) = \int_{x_2}^{x_1} J(x; s) e^{sx} dx; \quad (121)$$

If the initial waveform $\phi_0(x)$ satisfies

$$\frac{d^{p+1}}{dx^{p+1}} \phi_0(x) < b_0 ; \quad (122)$$

then from integration by parts, we have

$$\int_{x_2}^{x_1} e^{sx} \phi_0(x) dx = \frac{1}{s} \int_{x_2}^{x_1} e^{sx} \frac{d}{dx} [\phi_0(x)] dx \quad (123)$$

$$= \frac{1}{s^{p+1}} \int_{x_2}^{x_1} e^{sx} \frac{d^{p+1}}{dx^{p+1}} [\phi_0(x)] dx \quad (124)$$

$$= \frac{1}{s^{p+1}} e^{sx_2} \int_{x_2}^{x_1} e^{s(x-x_2)} \frac{d^{p+1}}{dx^{p+1}} [\phi_0(x)] dx : \quad (125)$$

For $\text{Re}(s) > 0$ the factor $e^{s(x-x_2)}$ in the last integral is < 1 , so that

$$e^{sx_2} \int_{x_2}^{x_1} e^{sx} \phi_0(x) dx < \frac{\int_{x_2}^{x_1} \frac{d^{p+1}}{dx^{p+1}} [\phi_0(x)] dx}{s^{p+1}} : \quad (126)$$

If in addition to the constraint in (122) we have that the p^{th} derivative of $\phi_0(x)$ is bounded, then by a very similar argument we can show that $\phi(s)$, defined as $e^{sx_2} J(s)$, satisfies

$$|J(s)| < \frac{\text{const}}{|s|^{p+1}} : \quad (127)$$

We can now apply the above mathematical results to the Green function integral from Sec. III. The waveform is given by the following integral along the imaginary s axis:

$$\phi(t; x) = \frac{1}{2i} \int_{-\infty}^{\infty} \frac{e^{s(t-x)} J(s)}{W(s)} ds \quad (128)$$

where $W(s)$ is given in (57) & (60) and has the form $W(s) = s^2 e^{2sL} \phi(s)$ in which $\phi(s)$ is a special case of (79) and (80). We can therefore rewrite the solution as

$$\phi(t; x) = \frac{1}{2i} \int_{-\infty}^{\infty} \frac{s^2 e^{s(t-x+x_2+2L)} \phi(s)}{(s)} ds : \quad (129)$$

The above proof requires that p, d_1, d_2 and L satisfy the inequalities that follow (81). The details of the proof show that the rate of convergence depends on these parameters. In particular, on the value of $p + (3d_2 - 2L) - 2$. A small value of this parameter means slow convergence. We can now relate the details of the proof to the examples presented in Sec. III, and examine the interesting nature of the convergence of the series given there. We start by noting that a straightforward computation of $\phi(s) = e^{sx_2} J(s)$, for the Cauchy data of (19), shows that $p = 1$. Comparing (78) and (129) we see that

$$\begin{aligned} d_1 + d_2 &= t - x + x_2 + 2L \\ &= t - x + x_1 - x_1 + x_2 + 2L : \end{aligned} \quad (130)$$

An "obvious" choice is to take $d_1 = t - x + x_1$, the retarded time from the start of the reception of signals from the Cauchy data. At any x this is the equivalent of t_{min} . With this choice we are left with $d_2 = x_2 - x_1 + 2L$. (Note that $2L - d_2 = x_1 - x_2$ is positive, as required in the proof.) The value of p for this choice is given by

$$p + \frac{3d_2}{2L} - 2 = 2 - \frac{x_1 - x_2}{2L} : \quad (131)$$

In our examples, we choose $x_1 = x_2$, the range of support of the Cauchy data, to be 6 and we have $L = 9$, so p is unity. Suppose, though, that we had chosen $x_1 = 1$ (as in our standard sine wave data of Sec. III) but had decreased the value of x_2 below our standard choice -5. The details of the proof show that convergence would require more terms for a given level of accuracy and that the series would fail to converge for $x_2 < -11$. This limit can be extended if we use initial data with one or more continuous derivatives, i.e. if $p > 1$. This rather unusual feature was, in fact, exactly what was observed in numerical experiments.

We point out next that Lemma 3 shows that convergence is not uniform in d_1 . As d_1 gets smaller, more terms in the series are needed. With our choice of d_1 to be t_{min} , this implies that the convergence of our QN series in (83) is not uniform as $t_{\text{min}} \rightarrow 0$, contradicting our claims of uniform convergence made following (5). But note that we can choose $d_1 = t_{\text{min}} + 1$, so that convergence is uniform for $t > t_{\text{min}}$. In this case we have $\epsilon = 2 - 3(x_1 - x_2 + 1) = 2L$. For both our sine wave Cauchy data this has a numerical value of 5=6, and the series is convergent. It is clear that there is an interaction between the allowed range of the Cauchy data, and the range of t for which the QN series converges. By moving the left edge of the support of the Cauchy data to the left by some amount δ , we increase by $3\delta = (2L)$ the value of t at which the series first converges. It should also be noted that the dependence on d_1 explains why the QN series converge more quickly at early times than at late, a feature evident in Fig.9.

- [1] The following references contain examples of QN ringing in a variety of contexts, and contain references to further work: C. V. Vishveshwara, Nature 227, 936 (1970); W. H. Press, Astrophys. J. 170, L105 (1971); S. L. Detweiler and E. Szedenits, Jr., Astrophys. J. 231, 211 (1979); C. T. Cunningham, R. H. Price, and V. Moncrief, Astrophys. J. 236, 674 (1980); K. Oohara, Prog. Theor. Phys. 71, 738 (1984); R. F. Stark and T. Piran, Phys. Rev. Lett. 55, 891 (1985); 56, 97 (E) (1986); A. M. Abraham and C. R. Evans, Phys. Rev. D 46, R4117 (1992); P. Anninos, D. Hobill, E. Seidel, L. Smarr, W.-M. Suen, Phys. Rev. Lett. 71, 2851 (1993); R. Geiser, C. Nicasio, R. H. Price and J. Pullin, Class. Q. Grav. 13, L117 (1996).
- [2] H. R. Beyer, Max-Planck-Institut für Astrophysik preprint MPA 811 (1994); J. Math. Phys. 36, 4792-4814 (1995); J. Math. Phys. 36, 4815-4825 (1995).
- [3] H. R. Beyer and B. G. Schmidt, Astron. Astrophys. 296, 722-726 (1995).
- [4] E. S. C. Ching, P. T. Leung, W.-M. Suen and K. Young, Phys. Rev. Lett. 74, 4588-4591 (1995); Phys. Rev. D 54, 3778-3791 (1996).
- [5] T. Regge and J. A. Wheeler, Phys. Rev. 108, 1063 (1957).
- [6] F. J. Zerilli, Phys. Rev. Lett. 24, 737 (1970).
- [7] S. Chandrasekhar, The Mathematical Theory of Black Holes (Clarendon, Oxford, 1983).
- [8] H.-P. Nollert and B. G. Schmidt, Phys. Rev. D 45, 2617 (1992).
- [9] E. W. Leaver, Proc. R. Soc. London A 402, 285 (1985).
- [10] V. Husain and R. H. Price, Phys. Rev. Lett. 68, 1973 (1992).
- [11] G. Poschl and E. Teller, Z. Phys. 83, 143 (1933).
- [12] V. Ferrari and B. Mashhoon, Phys. Rev. Lett. 16, 1361 (1984).
- [13] H.-P. Nollert Phys. Rev. D 53, 4397 (1996).
- [14] R. H. Price and J. Pullin, Phys. Rev. Lett. 72, 3297 (1994).